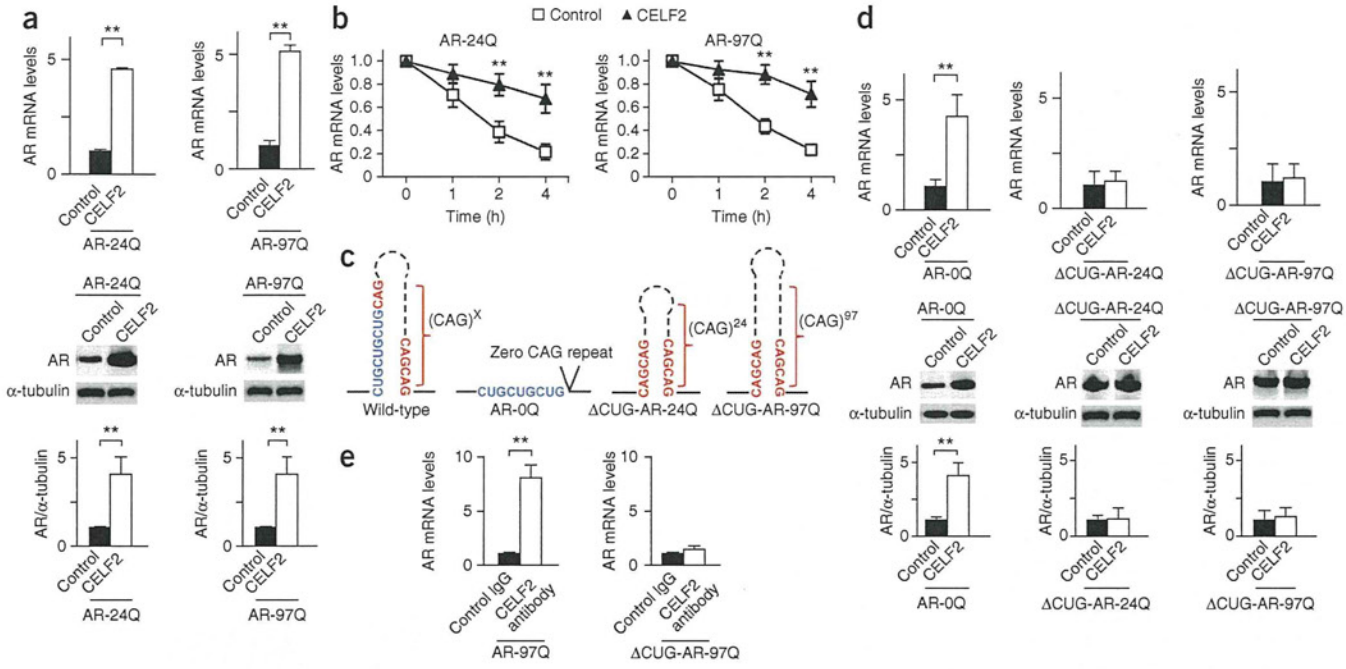


**Figure 2** CELF2 recognizes the sequence CUGCUGCUG in exon 1 of the AR mRNA and increases the stability of the AR mRNA. (**a**) The expression levels of AR mRNA and protein in HEK293T cells treated with the DNA plasmid expressing human CELF2 (CELF2) or the original pcDNA3.1/HisC vector (control) ($n = 5$). (**b**) RNA stability assays in HEK293T cells treated with CELF2 or control ($n = 5$). (**c**) Schematic diagrams of the AR mRNA structure near the hairpin loop of the CAG repeats (red) transcribed from wild-type and mutated DNA plasmids. AR-0Q lacks the CAG repeats, and ΔCUG-AR-24Q and ΔCUG-AR-97Q lack the sequence CUGCUGCUG (blue) immediately adjacent to the CAG repeats. (**d**) AR mRNA and protein expression levels in HEK293T cells co-transfected with CELF2 and the mutated DNA plasmids expressing AR ($n = 5$). (**e**) The amount of AR-97Q and ΔCUG-AR-97Q mRNA binding to CELF2 that was immunoprecipitated using an antibody against CELF2 or a control immunoglobulin (IgG) ($n = 5$). All data are means ± s.e.m. $^{**}P < 0.01$ (we analyzed the results by unpaired *t* tests in **a**,**d** and **e** and by two-way ANOVA followed by the Bonferroni test comparing HEK293T cells treated with CELF2 to cells treated with control in **b**).

a widespread transduction of the viral particles throughout the brain, spinal cord and the skeletal muscle of the upper and lower limbs was observed (**Supplementary Fig. 4a**). There was no difference in the expression of EGFP between the left and right sides of the spinal cord (**Supplementary Fig. 4b**). The presence of the AAV vector in the motor neurons of infected mice was visually confirmed by the colocalization of EGFP and staining for choline acetyltransferase (ChAT), a motor neuron marker (**Supplementary Fig. 4c**). Because the widespread viral transduction throughout the entire body was also detected in mice in which virus was injected into a cardiac chamber (**Supplementary Fig. 4d**), we deduced that the viral particles injected into the hind limb skeletal muscle spread hematogenously throughout the entire body of the mouse. In addition to viral distribution, a tyrosine mutation of the adeno-associated viral capsid protein may contribute to the enhanced transgene expression levels delivered by AAV[23]. We then did an AAV vector injection into the quadriceps femoris of a 5-week-old mouse, before the onset of motor impairment in the SBMA mice (approximately 7 weeks of age), because transgene expression stabilizes approximately 2 weeks after vector delivery.

The disease progression in the AR-97Q mice treated with AAV-miR-196a (AR-97Q-miR-196a mice) was ameliorated compared with AAV-miR-mock-treated mice. The AR-97Q mice treated with AAV-miR-mock (AR-97Q-miR-mock mice) showed motor impairment, as assessed by the rotarod task, as early as 7 weeks after birth. By contrast, the AR-97Q-miR-196a mice showed an initial impairment at 13 weeks after birth but showed less deterioration than their AR-97Q-miR-mock counterparts ($P < 0.001$) (**Fig. 3a**). The locomotor cage activity of the AR-97Q-miR-mock mice was also markedly decreased at 7 weeks compared with that of the AR-97Q-miR-196a mice ($P < 0.001$), which showed decreased activity at 13 weeks of age (**Fig. 3b**). Moreover, the AR-97Q-miR-mock mice lost weight significantly earlier and more profoundly than the AR-97Q-miR-196a mice ($P < 0.001$) (**Fig. 3c**). Treatment with miR-196a significantly prolonged the survival of the AR-97Q-miR-196a mice ($P < 0.001$) compared with the AR-97Q-miR-mock mice (**Fig. 3d**). By 12 weeks of age, the AR-97Q-miR-mock mice showed obvious differences in body size, muscular atrophy and kyphosis compared with the AR-97Q-miR-196a mice (**Fig. 3e**). In addition, the AR-97Q-miR-mock mice showed motor weakness, as indicated by short steps and leg dragging, whereas the AR-97Q-miR-196a mice showed almost normal ambulation (**Fig. 3f**). Immunohistochemical examination of mouse tissues using 1C2 antibody, which specifically recognizes the expanded polyQ region in the mutant AR, showed a marked reduction in 1C2-positive nuclear accumulation in the anterior horn of the thoracic spinal cord and in the skeletal muscles of the right quadriceps femoris of the AR-97Q-miR-196a mice compared with those of the AR-97Q-miR-mock mice. Glial fibrillary acidic protein (GFAP)-specific antibody staining showed that the AAV vector–mediated delivery of miR-196a reduced reactive astrogliosis in the thoracic spinal anterior horn of the AR-97Q mice, thereby suggesting that miR-196a attenuated neurodegenerative changes. Histopathological examination of the skeletal muscle showed marked amelioration of neurogenic muscle atrophy in the AR-97Q-miR-196a mice compared with the AR-97Q-miR-mock mice (**Fig. 3g**). By quantitative assessment, we confirmed that AAV-miR-196a significantly reduced 1C2-positive nuclear accumulation in the anterior horn of the thoracic spinal cord ($P < 0.01$) and

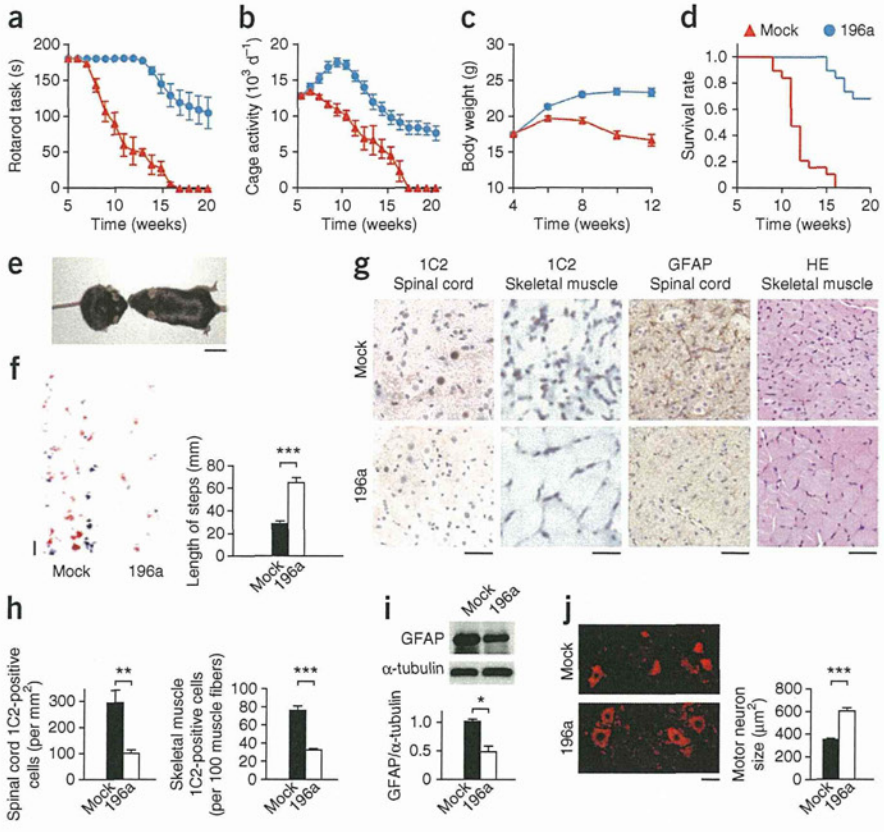


**Figure 3** The effects of miR-196a on the phenotype of male AR-97Q mice. (**a**–**d**) A rotarod task (**a**), cage activity (**b**), body weight (**c**) and survival rate (Kaplan-Meier analysis and log-rank test) (**d**) of the AR-97Q-miR-mock (mock) or AR-97Q-miR-196a mice (196a) ($n = 19$ in each group). $P < 0.001$ for all data at each time after 8 weeks of age in **a**–**c**. (**e**,**f**) A representative photograph (**e**) and footprints (**f**) of a 12-week-old AR-97Q-miR-mock mouse (left) and an age-matched AR-97Q-miR-196a mouse (right). The front and hind paws are indicated in red and blue, respectively. Each column shows the average length of the steps taken by the hind paw ($n = 5$). Scale bars, 20 mm. (**g**) Immunohistochemical staining for the mutant AR using the 1C2 antibody of the thoracic spinal cord and skeletal muscle of the right quadriceps femoris; immunohistochemical staining with a GFAP-specific antibody of the thoracic spinal anterior horn; and hematoxylin and eosin (HE) staining of the skeletal muscle of the right quadriceps femoris. Scale bars, left to right: 50 μm, 10 μm, 50 μm, 20 μm. (**h**) Quantification of 1C2-positive cells in the thoracic spinal cord and skeletal muscle of the right quadriceps femoris ($n = 5$). (**i**) Western blot and densitometric analyses showing the levels of GFAP protein expression in the thoracic spinal cord ($n = 5$). (**j**) The mean size of the motor neurons of the thoracic spinal cord obtained from AR-97Q-miR-196a mice compared with that of AR-97Q-miR-mock mice ($n = 5$). Scale bar, 20 μm. All data are means ± s.e.m. $^*P < 0.05$, $^{**}P < 0.01$ and $^{***}P < 0.001$ (we analyzed the results by two-way ANOVA followed by the Bonferroni test comparing the mock to 196a in **a**–**c** and by unpaired *t* test in **f**, **h**–**j**).

in the skeletal muscle of the right quadriceps femoris ($P < 0.001$) of the AR-97Q-mice (**Fig. 3h**). Western blot analyses and quantification of the immunohistochemical signal intensities revealed that treatment with miR-196a downregulated the expression levels of GFAP (**Fig. 3i** and **Supplementary Fig. 5**). In addition, treatment with miR-196a significantly suppressed motor neuron shrinkage ($P < 0.001$) (**Fig. 3j**).

At 3 weeks after injection of a viral load of $10^{11}$ vg, we killed the mice and harvested the RNA and protein in the thoracic spinal cord for analysis. The AR-97Q-miR-196a mice showed high expression levels of miR-196a and low expression levels of CELF2 mRNA, mutant AR mRNA and the endogenous mouse AR mRNA in the thoracic spinal cord compared with AR-97Q-miR-mock mice (**Fig. 4a**). The mouse AR mRNA lacks a CUGCUGCUG tract; however, it has the CUGCUG sequence in its coding region that would interact with CELF2. Western blotting analyses of thoracic spinal cord lysates of the AR-97Q-miR-mock mice showed that the high-molecular-weight mutant AR protein complex was retained in the stacking gel and that a monomeric AR migrated as a band through the separating gel (**Fig. 4b**). Treatment with AAV-miR-196a notably reduced both the high-molecular-weight complex and the monomer of AR and CELF2 in the thoracic spinal cord (**Fig. 4b**). We observed the elevated expression levels of miR-196a achieved by AAV vector–mediated expression and the decreased expression levels of mutant AR mRNA in the thoracic spinal cord throughout the follow-up period of 15 weeks (**Fig. 4c**). Although we detected the effects of the miR-196a treatment in the skeletal muscle, we found that the increase in the levels of miR-196a expression and the downregulation of mutant AR mRNA and protein were more prominent in the spinal cord than in the skeletal muscle (**Supplementary Fig. 6**). The skeletal muscle of the right quadriceps femoris, contralateral to the site of the AAV vector injection, also showed treatment effects (**Supplementary Fig. 6**). AR-97Q-miR-196a mice showed no detectable reduction in the normal serum testosterone levels, which has been shown to directly affect the levels of AR expression (**Fig. 4d**)[11].

To address whether miR-196a-mediated treatment can be useful in the therapy of patients with SBMA, we examined the effects of miR-196a on AR mRNA and protein in fibroblasts obtained from patients with SBMA and from disease control subjects. Treatment with miR-196a downregulated both the AR and CELF2 mRNAs and proteins in the fibroblasts obtained from patients with SBMA (**Fig. 4e**) and disease control subjects (**Supplementary Fig. 7**). We also observed similar effects for AR mRNA and protein in fibroblasts treated with CELF2 siRNA (**Fig. 4f**). Taken together, these findings suggest that miR-196a-mediated treatment might be useful in the therapy of patients with SBMA. Furthermore, we measured the expression levels of miR-196a, miR-196b and CELF2 mRNA in the thoracic spinal cord of patients with SBMA. Both of the two miRNAs were upregulated and the CELF2 mRNA was downregulated in the thoracic spinal cord of patients with SBMA compared with those of disease control subjects (**Fig. 4g**). qRT-PCR revealed that the expression levels of CELF2 mRNA were lower in the thoracic spinal cord of AR-97Q mice than in AR-24Q mice (**Supplementary Fig. 8**), thereby confirming the correlations between the *in vivo* levels of the two miRNAs and CELF2 mRNA. We also showed the *in vivo* correlation between miR-196a and mutant AR mRNA levels and monitored the side effects of mice treated with AAV-miR-196a (**Supplementary Note**

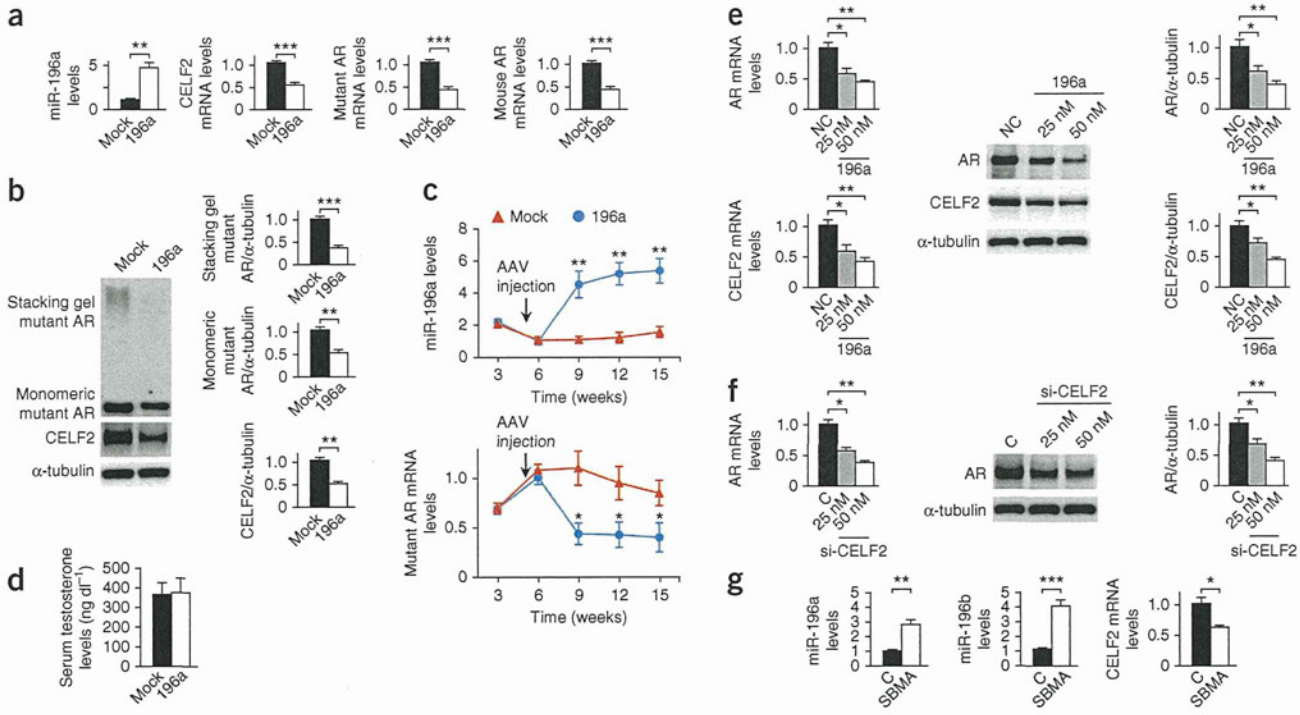


**Figure 4** The effects of miR-196a on mutant AR expression in male AR-97Q mice and patients with SBMA. **(a)** The levels of miR-196a, CELF2 mRNA, mutant AR mRNA and the endogenous mouse AR mRNA expression in the thoracic spinal cord of AR-97Q-miR-mock (mock) and AR-97Q-miR-196a (196a) mice ($n = 5$). **(b)** Western blot and densitometric analyses showing the expression levels of mutant AR both in the stacking and separating gels as well as those of CELF2 ($n = 5$). **(c)** A temporal change in the levels of miR-196a and mutant AR mRNA expression in the thoracic spinal cord of AR-97Q-miR-mock and AR-97Q-miR-196a mice ($n = 3$ to 4). **(d)** The serum testosterone levels of AR-97Q-miR-mock and AR-97Q-miR-196a mice ($n = 5$). **(e)** The expression levels of mutant AR mRNA, CELF2 mRNAs and their proteins in the fibroblasts of patients with SBMA ($n = 5$). NC, a negative control miRNA. **(f)** The effects of CELF2 silencing on mutant AR mRNA and protein in the fibroblasts of patients with SBMA ($n = 5$). C, a scrambled control siRNA. **(g)** The expression levels of miR-196a, -196b and CELF2 mRNA in the thoracic spinal cord of patients with SBMA ($n = 3$). C, disease control subjects. All data are means ± s.e.m. $^*P < 0.05$, $^{**}P < 0.01$ and $^{***}P < 0.001$ (we analyzed the results by unpaired *t* tests in **a**,**b**,**d** and **g** and by two-way ANOVA followed by the Bonferroni test comparing the mock to 196a in **c**, and by the Dunnett test in **e**,**f**).

and **Supplementary Fig. 8**). In addition, we examined the post-translational effects of miR-196a in HEK293T and the effects of miR-196a on apoptosis in Neuro2a cells (**Supplementary Note** and **Supplementary Fig. 9**). We also showed the effects of miR-196a downregulation on mutant AR mRNA and protein in HEK293T cells (**Supplementary Note** and **Supplementary Fig. 10**).

In this study, we showed that miR-196a is upregulated in the spinal cord of a transgenic mouse model of SBMA during the symptomatic stage and that early intervention by the transduction of mice with miR-196a via an AAV vector can markedly ameliorate the motor impairment of SBMA mice. We further showed that miR-196a silences CELF2, which then directly acts on AR mRNA to affect its stability. Although polyQ models have been shown to have altered miRNA profiles[7,17] and miRNAs targeting of the polyQ disease gene have been proposed as disease modifiers [6,7], the miRNA-mediated therapeutic approach targeting a regulator of the disease transcript described in our study is conceptually novel and could be strategically applied to other polyQ-related diseases.

The upregulation of miR-196a has been reported in a wide variety of cancers[24,25] and has also been shown to be involved in differentiation[26,27] and the development of the immune system[28]. Hence, miR-196a has previously been proposed as a therapeutic target for these ailments. Similarly, the modulation of CELF2 has known implications for myotonic dystrophy[29] and several cancer types[30,31].

Our results show that the strong and continuous inhibition of the expression of CELF2 by the AAV vector–mediated delivery of miR-196a has a substantial effect on the SBMA phenotype. Although the reason for the natural upregulation of miR-196a in the spinal cord of SBMA mice and patients with SBMA is unknown, it may indicate a protective mechanism that is insufficient alone but sufficiently beneficial when amplified by AAV-mediated overexpression. However, whether similarly effective therapy would result from injections to an isolated skeletal muscle in patients with SBMA must be verified. The appropriate route and the required dose of AAV administration should be determined in future studies. Our findings indicate that the miRNA-mediated regulation of RNA metabolism is a logical target for the therapeutic intervention of SBMA and they suggest a new therapeutic approach using an AAV vector–mediated miRNA delivery system for the treatment of neurodegenerative disease.

## METHODS

Methods and any associated references are available in the online version of the paper.

*Note: Supplementary information is available in the online version of the paper.*

ACKNOWLEDGMENTS

We are grateful to T. Cooper (Department of Pathology and Immunology, Baylor College of Medicine) for kindly providing the plasmid expressing human CELF2. We also thank N. Takino, H. Miyauchi and K. Ayabe (Division of Neurology, Department of Medicine, Jichi Medical University) for their help with the production of the AAV vectors and Y. Kondo and K. Shinjo (Division of Molecular Oncology, Aichi Cancer Center Research Institute) for expert technical support and helpful discussions. This work was supported by grants from the Ministry of Health,

Labor and Welfare; grants from the Ministry of Education, Culture, Sports, Science, and Technology of Japan; a Center-of-Excellence (COE) grant; a Grant-in-Aid for Scientific Research on Innovated Areas "Foundations of Synapse and Neurocircuit Pathology"; and the Core Research for Evolutional Science and Technology (CREST) program of the Japan Science and Technology Agency (JST).

AUTHOR CONTRIBUTIONS

Project planning was done by Y.M., H.A., M.K., F.T., S. Muramatsu and G.S.; experimental work was done by Y.M., H.A., M.K., M.M., Y.-M.J., Z.H., H.D., S. Matsumoto, N.K., M.I., G.T. and S. Muramatsu; data analysis was done by Y.M., H.A., M.K., F.T., S. Muramatsu and G.S.; the manuscript was written by Y.M., H.A., M.K., F.T., S. Muramatsu and G.S.

COMPETING FINANCIAL INTERESTS

The authors declare no competing financial interests.

Published online at http://www.nature.com/doifinder/10.1038/nm.2791.
Reprints and permissions information is available online at http://www.nature.com/reprints/index.html.

1. La Spada, A.R., Wilson, E.M., Lubahn, D.B., Harding, A.E. & Fischbeck, K.H. Androgen receptor gene mutations in X-linked spinal and bulbar muscular atrophy. *Nature* **352**, 77–79 (1991).
2. Kennedy, W.R., Alter, M. & Sung, J.H. Progressive proximal spinal and bulbar muscular atrophy of late onset: a sex-linked recessive trait. *Neurology* **50**, 583–593 (1998).
3. Sobue, G. *et al.* X-linked recessive bulbospinal neuronopathy. A clinicopathological study. *Brain* **112**, 209–232 (1989).
4. Kim, V.N., Han, J. & Siomi, M.C. Biogenesis of small RNAs in animals. *Nat. Rev. Mol. Cell Biol.* **10**, 126–139 (2009).
5. Kim, J. *et al.* A MicroRNA feedback circuit in midbrain dopamine neurons. *Science* **317**, 1220–1224 (2007).
6. Karres, J.S., Hilgers, V., Carrera, I., Treisman, J. & Cohen, S.M. The conserved microRNA miR-8 tunes atrophin levels to prevent neurodegeneration in *Drosophila*. *Cell* **131**, 136–145 (2007).
7. Lee, Y. *et al.* miR-19, miR-101 and miR-130 co-regulate ATXN1 levels to potentially modulate SCA1 pathogenesis. *Nat. Neurosci.* **11**, 1137–1139 (2008).
8. Williams, A.H. *et al.* MicroRNA-206 delays ALS progression and promotes regeneration of neuromuscular synapses in mice. *Science* **326**, 1549–1554 (2009).
9. Roshan, R., Ghosh, T., Scaria, V. & Pillai, B. MicroRNAs: novel therapeutic targets in neurodegenerative diseases. *Drug Discov. Today* **14**, 1123–1129 (2009).
10. Boudreau, R.L., Rodríguez-Lebrón, E. & Davidson, B.L. RNAi medicine for the brain: progresses and challenges. *Hum. Mol. Genet.* **20**, R21–R27 (2011).
11. Katsuno, M. *et al.* Testosterone reduction prevents phenotypic expression in a transgenic mouse model of spinal and bulbar muscular atrophy. *Neuron* **35**, 843–854 (2002).
12. Katsuno, M. *et al.* Leuprorelin rescues polyglutamine-dependent phenotypes in a transgenic mouse model of spinal and bulbar muscular atrophy. *Nat. Med.* **9**, 768–773 (2003).
13. Adachi, H. *et al.* Heat shock protein 70 chaperone overexpression ameliorates phenotypes of the spinal and bulbar muscular atrophy transgenic mouse model by reducing nuclear-localized mutant androgen receptor protein. *J. Neurosci.* **23**, 2203–2211 (2003).
14. Waza, M. *et al.* 17-AAG, an Hsp90 inhibitor, ameliorates polyglutamine-mediated motor neuron degeneration. *Nat. Med.* **11**, 1088–1095 (2005).
15. Tokui, K. *et al.* 17-DMAG ameliorates polyglutamine-mediated motor neuron degeneration through well-preserved proteasome function in an SBMA model mouse. *Hum. Mol. Genet.* **18**, 898–910 (2009).
16. Eacker, S.M., Dawson, T.M. & Dawson, V.L. Understanding microRNAs in neurodegeneration. *Nat. Rev. Neurosci.* **10**, 837–841 (2009).
17. Bilen, J., Liu, N., Burnett, B.G., Pittman, R.N. & Bonini, N.M. MicroRNA pathways modulate polyglutamine-induced neurodegeneration. *Mol. Cell* **24**, 157–163 (2006).
18. Schaefer, A. *et al.* Cerebellar neurodegeneration in the absence of microRNAs. *J. Exp. Med.* **204**, 1553–1558 (2007).
19. Kaspar, B.K. *et al.* Retrograde viral delivery of IGF-1 prolongs survival in a mouse ALS model. *Science* **301**, 839–842 (2003).
20. Towne, C. *et al.* Efficient transduction of non-human primate motor neurons after intramuscular delivery of recombinant AAV serotype 6. *Gene Ther.* **17**, 141–146 (2010).
21. Dominguez, E. *et al.* Intravenous scAAV9 delivery of a codon-optimized SMN1 sequence rescues SMA mice. *Hum. Mol. Genet.* **20**, 681–693 (2011).
22. Fu, H., Dirosario, J., Killedar, S., Zaraspe, K. & McCarty, D.M. Correction of neurological disease of mucopolysaccharidosis IIIB in adult mice by rAAV9 trans-blood-brain barrier gene delivery. *Mol. Ther.* **19**, 1025–1033 (2011).
23. Petrs-Silva, H. *et al.* Novel properties of tyrosine-mutant AAV2 vectors in the mouse retina. *Mol. Ther.* **19**, 293–301 (2011).
24. Hui, A.B. *et al.* Robust global micro-RNA profiling with formalin-fixed paraffin-embedded breast cancer tissues. *Lab. Invest.* **89**, 597–606 (2009).
25. Maru, D.M. *et al.* MicroRNA-196a is a potential marker of progression during Barrett's metaplasia-dysplasia-invasive adenocarcinoma sequence in esophagus. *Am. J. Pathol.* **174**, 1940–1948 (2009).
26. Yekta, S., Shih, I.H. & Bartel, D.P. MicroRNA-directed cleavage of HOXB8 mRNA. *Science* **304**, 594–596 (2004).
27. Hornstein, E. *et al.* The microRNA miR-196 acts upstream of Hoxb8 and Shh in limb development. *Nature* **438**, 671–674 (2005).
28. Pedersen, I.M. *et al.* Interferon modulation of cellular microRNAs as an antiviral mechanism. *Nature* **449**, 919–922 (2007).
29. Dhaenens, C.M. *et al.* Mis-splicing of *Tau* exon 10 in myotonic dystrophy type 1 is reproduced by overexpression of CELF2 but not by MBNL1 silencing. *Biochim. Biophys. Acta* **1812**, 732–742 (2011).
30. Natarajan, G. *et al.* CUGBP2 downregulation by prostaglandin E2 protects colon cancer cells from radiation-induced mitotic catastrophe. *Am. J. Physiol. Gastrointest. Liver Physiol.* **294**, G1235–G1244 (2008).
31. Subramaniam, D. *et al.* RNA binding protein CUGBP2/CELF2 mediates curcumin-induced mitotic catastrophe of pancreatic cancer cells. *PLoS ONE* **6**, e16958 (2011).

## ONLINE METHODS

**Construction of DNA plasmids.** We constructed cDNA expression plasmids encoding full-length AR by subcloning AR cDNA derived from pSP64-AR24 and pSP64-AR97 (ref. 32) into the pCR3.1 mammalian expression vector (Life Technologies). We carried out an L55 L56 L57 (CTGCTGCTG) deletion of AR-24Q and AR-97Q as follows: the pBS+AflII plasmid was generated by the insertion of an AflII linker into the EcoRV site of pBluescript II KS(−). We excised the 417-bp fragment of 24Q and the 636-bp fragment of 97Q from pCR3.1-AR-24Q and -97Q using SmaI and AflII and cloned it into the SmaI and AflII sites of pBS+AflII to create pBS-24Q and -97Q. pBS-ΔCUG-24Q and -97Q were constructed by inserting the double-stranded oligomer CCAGTTTGCA into pBS-24Q and -97Q digested with NarI-PstI (blunted). Finally, we re-excised the pBS-ΔCUG-24Q and -97Q with SmaI-AflII and inserted this fragment between the SmaI and AflII sites of pCR3.1-AR to form pCR3.1-AR ΔCUG-24Q and -97Q.

The CAG repeat deletion of the AR construct was generated using a KOD-Plus-Mutagenesis kit (Toyobo) with the forward primer 5′-CAAGAG ACTAGCCCCAGGCAGCAGC-3′ and the reverse primer 5′-CAGCAGCA GCAAACTGGCGCCG-3′. The DNA plasmid expressing human CELF2 was kindly provided by T. Cooper (Professor, Department of Pathology and Immunology, Baylor College of Medicine). The siRNA-resistant construct was generated by changing the siRNA targeted sequence (5′- GAATGCACTGCACA ATATT -3′) of pcDNA3.1/HisC-CELF2 to 5′- AAACGCGCTACATAACATC -3′ (mutated nucleotides are underlined) using a KOD-Plus-Mutagenesis kit (Toyobo) with the forward primer 5′-ACATAACATCAAAACTTTACCTGG GATGCATCATCCCA-3′ and the reverse primer 5′-AGCGCGTTTTGGGCC TCAAGTGCAGCTTTTCTTGTATA-3′. The sequences of all mutations and the CAG repeat length were confirmed using a CEQ 8000 Genetic Analysis System (Beckman Coulter). We used the original pcDNA3.1/HisC vector lacking the insertions in the multiple cloning sites as a mock vector.

**Co-transfection of DNA plasmids with either synthetic miRNA or siRNA into cultured cells.** The sequences of the siRNA target for CELF2 mRNA are 5′-GAATGCACTGCACAATATT-3′ (accession number NM_001025076), 5′-CACCTATCGTGGTGAAGTT-3′ (accession number NM_001025076) and 5′- CACAGTATCTGGCGCTCCT-3′ (accession number NM_001025076). All of the siRNAs were purchased from Sigma-Aldrich. A scrambled control siRNA (MISSION siRNA Universal Negative Control SIC-001; Sigma-Aldrich), synthetic miR-196a (MISSION microRNA Mimics -hsa-miR-196a; Sigma-Aldrich), synthetic miR-196b (MISSION microRNA Mimics -hsa-miR-196b; Sigma-Aldrich), synthetic miR-496 (MISSION microRNA Mimics -hsa-miR-496; Sigma-Aldrich), synthetic miR-323-3p (MISSION microRNA Mimics -hsa-miR-323-3p; Sigma-Aldrich), synthetic miR-29b* (Syn-mmu-miR-29b-1* miScript miRNA Mimic; Qiagen), anti-miR-196a antisense (anti-hsa-miR-196a miScript miRNA Inhibitor; Qiagen) and negative control miRNA (MISSION microRNA Mimic, Human, Negative Control 1; Sigma-Aldrich) were purchased. We plated HEK293T cells onto six-well dishes and co-transfected each dish with 0.5 μg of the vector containing the following: AR-24Q, AR-97Q, ΔCUG-AR-24Q, ΔCUG-AR-97Q or AR-0Q; 2.0 μg of the vector containing CELF2, siRNA-resistant CELF2 or mock; and either 25 nM synthetic miRNA or 25 nM siRNA molecules. We used Lipofectamine 2000 (Life Technologies) as a transfection reagent in the cases in which all of the RNAi molecules purchased from Sigma-Aldrich were transfected into the HEK293T cells or Neuro2a cells. For the transfection of synthetic miR-29b* (Syn-mmu-miR-29b-1* miScript miRNA Mimic; Qiagen) and anti-miR-196a antisense (anti-hsa-miR-196a miScript miRNA Inhibitor; Qiagen) into HEK293T cells, we used the Attractene Transfection Reagent (Qiagen) as a transfection reagent. Neither the scrambled control siRNA nor the negative control miRNA matched any human or mouse mRNA. For the transfection of all of the RNAi molecules purchased from Sigma-Aldrich into human fibroblasts, we used jetPRIME (Polyplus-transfection SA) as a transfection reagent with a high amount of RNAi molecules because the human fibroblasts exhibited a lower transduction efficiency of RNAi molecules compared with those of the HEK293T cells and Neuro2a cells, for which we used Lipofectamine 2000 (Life Technologies) as a transfection reagent. The transfected cells were cultured for 48 h before being processed for western blotting and RNA analysis.

**Protein expression analysis.** We did western blotting and densitometric analyses as previously described[12,14]. We used the following primary antibodies: AR-specific antibody (1:5,000, N20 or 1:5,000, H280; Santa Cruz), CELF2-specific antibody (1:5,000, ab50734; Abcam), α-tubulin–specific antibody (1:5,000, T9026; Sigma-Aldrich), GFP-specific antibody (1:5,000, M048-3; MBL), GFAP-specific antibody (1:2,000, 814369; Boehringer Manheim Biochemica), IGF-1–specific antibody (1:1,000, ab9572; Abcam) and cleaved caspase-3–specific antibody (1:2,000, 9661s; Cell Signaling Technology).

**Quantitative real-time PCR.** For cultured cells, the total RNA was extracted from HEK293T cells using the QIAzol Lysis Reagent (Qiagen) and reverse transcribed using Superscript VILO (Life Technologies). The complementary DNAs were then used for real time PCR using the SsoFast EvaGreen Supermix (Bio-Rad Laboratories). For mouse tissue analysis, the total RNA was isolated from the thoracic spinal cord and skeletal muscles of mice using the QIAzol Lysis Reagent (Qiagen) and reverse transcribed with the miScript Reverse-Transcription Kit (Qiagen). The complementary DNAs were then used for real time PCR using the SYBR Green Supermix (Qiagen). We did the amplification, detection and data analysis using a Bio-Rad iCycler system (Bio-Rad Laboratories). The crossing threshold values for the mRNAs of the individual genes were normalized to β-2-microglobulin (B2MG). The crossing threshold values for the miRNA of the individual genes were normalized to the U6 small nuclear RNA 2. Changes in the expression of mRNA and miRNA were expressed as a fold change relative to the control.

We used the following primers in this study. The sequences of the hsa-AR primers were: forward, 5′-GGCTATGAATGTCAGCCCAT-3′; reverse, 5′-TTGAGG CTAGAGAGCAAGGC-3′. These hsa-AR primers discriminated between the human AR mRNA and the mouse AR mRNA. The sequences of the mmu-AR primers were: forward, 5′-TGGGACCTTGGATGGAGAACTA-3′; reverse, 5′-ACAGATCAGGCAGGTCTTCTGG-3′. These mmu-AR primers discriminated between the mouse AR mRNA and the human AR mRNA. The sequences of the hsa-CELF2 primers were: forward, 5′-CTGGCGGGAAACAAACTCTG-3′; reverse, 5′-TCTAAGCCCTTGGCCTCCTC-3′. The sequences of the mmu-CELF2 primers were: forward, 5′-GCTGTGCGTTTGTCACATTTTC-3′; reverse, 5′-TGTCAGC AAACTTCACCACGAT-3′. The sequences of the hsa-B2MG primers were: forward, 5′-CTGAAGCTGACAGCATTCGG-3′; reverse, 5′-GTCAACTTCAATGT CGGATGGATG-3′. The sequences of the mmu-B2MG primers were: forward, 5′-AAGCCGAACATACTGAACTGC-3′; reverse, 5′-GTGTGAGCCAGGATATA GAAAGAC-3′. The sequences of the hsa-IGF-1 primers were: forward, 5′-GCTGT GATCTAAGGAGGCTGGA-3′; reverse, 5′- TTCCTGCACTCCCTCTACTTGCA TGGATG-3′. The primers used for the detection of miR-196a, miR -196b and U6 small nuclear RNA 2 were the Hs_miR-196a_1 miScript Primer Assay (Qiagen), the Hs_miR-196b_2 miScript Primer Assay (Qiagen) and the Hs_RNU6-2_1 miScript Primer Assay (Qiagen), respectively.

**Immunoprecipitation-coupled qRT-PCR.** We did coimmunoprecipitation using an affinity-purified CELF2 antibody (15 μg per sample, ab50734; Abcam) followed by RNA isolation using the RiboCluster Profiler RIP-Assay kit (MBL International Corporation) according to the manufacturer's suggested protocols. Rabbit immunoglobulin G, supplied by the manufacturer, was used as a control, and the immunoprecipitated RNA was converted to cDNA using Superscript VILO (Life Technologies) and analyzed by qRT-PCR for the differential expression of AR mRNA using the following primers: forward, 5′-GGCTATGAATGTCAGCCCAT-3′; reverse, 5′-TTGAGGCT AGAGAGCAAGGC-3′.

**RNA stability assay.** We added actinomycin D (10 mg $ml^{-1}$ final concentration), a potent inhibitor of mRNA synthesis, to the HEK293T cells at 24 h after co-transfection of DNA plasmid and RNAi molecules. The total RNA was extracted from the cells at 0–4 h after treatment, and the RNA was then subjected to qRT-PCR as described above. The data are presented as values relative to the levels of expression detected in the transfected cells harvested at the time of actinomycin D treatment.

**miRNA microarray analysis.** The total RNA was extracted from the thoracic spinal cord of transgenic SBMA mice (AR-97Q) and wild-type mice (AR-24Q)


doi:10.1038/nm.2791

at 15 weeks of age and used for the miRNA microarray analysis conducted by TaKaRa Bio. Each group consisted of two mice.

**miRNA *in situ* hybridization.** To investigate the cell-specific distribution of miRNA in mouse spinal tissues, we did *in situ* hybridization using 5′- and 3′-end digoxigenin (DIG)-labeled locked nucleic acid (LNA)-modified DNA oligonucleotides complementary to the mature miRNA (Exiqon). In this study, we examined the global expression of miR-196a in mouse tissue sections that had been prepared as previously described[13–15,33]. The LNA-miR-196a and LNA-scrambled oligonucleotides (negative control) were used in this analysis.

We did the *in situ* hybridization of mouse tissue sections using a Ventana Discovery system (Ventana Medical Systems). Briefly, 5′- and 3′-end DIG-labeled LNA probes were stained with digoxigenin-AP–specific Fab fragments (1:800, 1093274; Roche). The sections were then counterstained using Red Counterstain II (780-2218; Ventana), and the signals were visualized under a standard light microscope.

**Development of the AAV vector with simultaneous expression of miRNA and EGFP.** The AAV vector plasmids contained an expression cassette consisting of a human cytomegalovirus immediate-early promoter, followed by cDNA encoding EGFP, miR-196a or the miR-mock sequence, and a woodchuck hepatitis virus post-transcriptional regulatory element between the inverted terminal repeats of the AAV3 genome. We synthesized the AAV9 *vp* cDNA, and this sequence was identical to that previously described[34] except for the substitution of adenine with thymidine at position 1337, which introduced an amino acid change from tyrosine to phenylalanine at position 446 (ref. 23). The recombinant AAV vectors were produced by transient transfection of HEK293 cells using the vector plasmid, an AAV3 *rep* and AAV9 *vp* expression plasmid and an adenoviral helper plasmid, pHelper (Stratagene), as previously described[35]. We purified the recombinant viruses by isolation from two sequential continuous CsCl gradients, and then the viral titers were determined by qRT-PCR. The cDNA sequences of miR-196a and miR-mock are as follows. miR-196a: 5′-TGAGCCGGGACTGTTGAGTGAAGTAGGT AGTTTCATGTTGTTGGGCCTGGCTTTCTGAACACAACGACATCAAA CCACCTGATTCATGGCAGTTACTGCTTC-3′. miR-mock: 5′-GTATTGC GTCTGTACACTCACCGTTTTGGCCACTGACTGACGGTGAGTGCAG ACGCAATA-3′.

**The neurological and behavioral assessment of the SBMA model mice.** We generated and maintained the AR-24Q and AR-97Q mice as previously described[12]. All of the animal experiments were carried out in accordance with the National Institutes of Health Guide for the Care and Use of Laboratory Animals and were approved by the Nagoya University Animal Experiment Committee. We did the mouse rotarod task and cage activity assessment as described previously[12,14]. The investigators who carried out the behavioral assessments were blinded to the treatment conditions.

**Immunohistochemistry, immunofluorescence, histochemistry and histopathology.** The preparation of the tissue sections, immunohistochemistry, immunofluorescence and histopathology were done as previously described[11–15, 33].

To quantify the 1C2-positive cells, we counted the 1C2-positive cells within the thoracic spinal cord and quadriceps femoris muscle for each individual mouse as previously described[12,14]. For choline acetyltransferase immunolabeling, the sections were first microwaved for 20 min in 50 mM citrate buffer, pH 6.0. For polyglutamine (1C2 antibody) immunolabeling, the sections were treated with formic acid for 5 min at room temperature. We treated all of the specimens with TNB blocking buffer (PerkinElmer) before incubation with primary antibodies. The immunohistochemical sections were then imaged using an optical microscope (BX51, Olympus), and the immunofluorescent specimens were photographed using an upright microscope (LSM710, Zeiss). We used the following primary antibodies: choline acetyltransferase–specific antibody (1:100, AB144; Millipore), mouse GFP-specific antibody (1:200, M048-3; MBL), mouse expanded polyQ antibody (1:10,000, 1C2; Millipore) and mouse GFAP-specific antibody (1:1,000, 814369; Boehringer Manheim Biochemica). The primary antibodies were probed with biotinylated anti–species-specific IgG secondary antibodies (Vector Laboratories), and the immune complexes were visualized using streptavidin–horseradish peroxidase (Dako) and 3,3′-diaminobenzidine as a substrate. We used Alexa-conjugated secondary antibodies (Life Technologies) for immunofluorescence. We assessed the size of the motor neuron in the thoracic spinal cord of the SBMA mice treated with AAV-miR-196a or AAV-miR-mock as previously described[33]. The stained sections were then examined and imaged using a BIOREVO BZ-9000 system (Keyence). To assess the GFAP expression levels in the thoracic spinal anterior horn cells, we quantified the immunohistochemistry signal intensities in at least ten transverse sections obtained from each mouse. The images of individual anterior horn on transverse sections of thoracic spinal cord with signals for GFAP were captured at the desired magnification and stored using image software (Keyence). The levels of GFAP staining in the images were quantitatively analyzed using image analysis software (Dynamic cell count BZ-HIC software, Keyence). The signal intensities were expressed as individual intracellular areas of GFAP staining ($\mu m^2$) in the unilateral thoracic spinal anterior horn.

**Assay of serum testosterone levels in SBMA mice.** We sacrificed SBMA mice treated with AAV-miR-196a or AAV-miR-mock at 12 weeks of age, collected 1 ml of blood by cardiocentesis and conducted an assay for serum testosterone levels using a radioimmunoassay (Mitsubishi Kagaku Bio-Clinical Laboratories).

**The fibroblasts and thoracic spinal cords of patients.** We obtained biopsy specimens of fibroblasts of scrotal skin from three patients genetically diagnosed with SBMA and three disease control subjects. The CAG repeat lengths of the patients with SBMA were 48, 50 and 52. The disease control subjects included three male individuals who were diagnosed with a cerebrovascular disease.

We obtained autopsy specimens of the thoracic spinal cord from three patients genetically diagnosed with SBMA (52-, 66- and 78-year-old males) and from disease control subjects (58-, 61- and 75-year-old males). The CAG repeat lengths of three patients with SBMA were 48, 49 and 50, respectively. The disease control subjects included individuals diagnosed with Parkinson's disease ($n = 2$) and dementia with Lewy body disease ($n = 1$). The collection of human tissues and their use for this study were approved by the Ethics Committee of Nagoya University Graduate School of Medicine. We obtained informed consent from the patients.

**The pulse-chase labeling assay.** HEK293T cells were transfected as previously described, starved for 1 h and then labeled for an additional 1 h with 150 mCi $ml^{-1}$ of EXPRE$^{35}$S$^{35}$S Protein Labeling Mix [$^{35}$S] (PerkinElmer Life & Analytical Sciences). We chased the HEK293T cells for the indicated time intervals. We then did immunoprecipitation using equivalent amounts of protein lysates as previously described[14] and analyzed the expression levels using phosphorimaging (Typhoon 8600 phosphorimager; Amersham) and Image Gauge software, version 4.22 (Fujifilm).

**The apoptosis assay.** We plated Neuro2a neuronal lineage cells onto six-well dishes and co-transfected each dish with 25 nM synthetic miR-196a using Lipofectamine 2000 (Life Technologies) according to the manufacturer's instructions. After 24 h, we treated the Neuro2a cells with 1 μM staurosporine, a major inducer of apoptosis, for 6 h. Next, we processed and probed the western blots with a cleaved caspase-3 antibody. The effect of miR-196a on apoptosis in the Neuro2a cells was then assessed by the change in the relative expression levels of cleaved caspase-3 protein.

**Statistical analyses.** We analyzed the results by unpaired *t* tests, Dunnett tests and two-way ANOVA followed by Bonferroni tests for individual paired comparison using IBM SPSS statistics version 19 for Windows (IBM). We used log-rank tests for the assessment of the survival rate in **Fig. 3d** using IBM

SPSS statistics version 19 for Windows (IBM). *P* values of less than 0.05 were considered statistically significant.


32. Kobayashi, Y. *et al.* Chaperones Hsp70 and Hsp40 suppress aggregate formation and apoptosis in cultured neuronal cells expressing truncated androgen receptor protein with expanded polyglutamine tract. *J. Biol. Chem.* **275**, 8772–8778 (2000).
33. Katsuno, M. *et al.* Disrupted transforming growth factor-β signaling in spinal and bulbar muscular atrophy. *J. Neurosci.* **30**, 5702–5712 (2010).
34. Gao, G. *et al.* Clades of adeno-associated viruses are widely disseminated in human tissues. *J. Virol.* **78**, 6381–6388 (2004).
35. Li, X.G. *et al.* Viral-mediated temporally controlled dopamine production in a rat model of Parkinson disease. *Mol. Ther.* **13**, 160–166 (2006).




doi:10.1038/nm.2791

OPEN ACCESS Freely available online

PLOS | ONE

# c-Abl Inhibition Delays Motor Neuron Degeneration in the G93A Mouse, an Animal Model of Amyotrophic Lateral Sclerosis

**Ryu Katsumata[1], Shinsuke Ishigaki[1,2,3], Masahisa Katsuno[1], Kaori Kawai[1], Jun Sone[1], Zhe Huang[1], Hiroaki Adachi[1], Fumiaki Tanaka[1], Fumihiko Urano[2,4], Gen Sobue[1,3]***

**1** Department of Neurology, Nagoya University Graduate School of Medicine, Tsurumai-cho, Showa-ku, Nagoya, Japan, **2** Program in Gene Function and Expression, University of Massachusetts Medical School, Worcester, Massachusetts, United States of America, **3** Core Research for Evolutional Science and Technology, Japan Science and Technology Agency, Saitama, Japan, **4** Program in Molecular Medicine, University of Massachusetts Medical School, Worcester, Massachusetts, United States of America

## Abstract

*Background:* Amyotrophic lateral sclerosis (ALS) is a fatal neurodegenerative disease characterized by progressive death of motor neurons. Although the pathogenesis of ALS remains unclear, several cellular processes are known to be involved, including apoptosis. A previous study revealed the apoptosis-related gene c-Abl to be upregulated in sporadic ALS motor neurons.

*Methodology/Findings:* We investigated the possibility that c-Abl activation is involved in the progression of ALS and that c-Abl inhibition is potentially a therapeutic strategy for ALS. Using a mouse motor neuron cell line, we found that mutation of Cu/Zn-superoxide dismutase-1 (SOD1), which is one of the causative genes of familial ALS, induced the upregulation of c-Abl and decreased cell viability, and that the c-Abl inhibitor dasatinib inhibited cytotoxicity. Activation of c-Abl with a concomitant increase in activated caspase-3 was observed in the lumbar spine of G93A-SOD1 transgenic mice (G93A mice), a widely used model of ALS. The survival of G93A mice was improved by oral administration of dasatinib, which also decreased c-Abl phosphorylation, inactivated caspase-3, and improved the innervation status of neuromuscular junctions. In addition, c-Abl expression in postmortem spinal cord tissues from sporadic ALS patients was increased by 3-fold compared with non-ALS patients.

*Conclusions/Significance:* The present results suggest that c-Abl is a potential therapeutic target for ALS and that the c-Abl inhibitor dasatinib has neuroprotective properties *in vitro* and *in vivo*.

**Citation:** Katsumata R, Ishigaki S, Katsuno M, Kawai K, Sone J, et al. (2012) c-Abl Inhibition Delays Motor Neuron Degeneration in the G93A Mouse, an Animal Model of Amyotrophic Lateral Sclerosis. PLoS ONE 7(9): e46185. doi:10.1371/journal.pone.0046185

**Editor:** Thomas H. Gillingwater, University of Edinburgh, United Kingdom

**Received** March 21, 2012; **Accepted** August 28, 2012; **Published** September 25, 2012



**Funding:** This work was supported by a Center-of-Excellence (COE) grant from the Ministry of Education, Culture, Sports, Science and Technology of Japan [http://w3serv.nagoya-u.ac.jp/coemed/en/index.html]; a Grant-in-Aid for Scientific Research on Innovated Areas "Foundation of Synapse and Neurocircuit Pathology" [http://www.tmd.ac.jp/mri/shingakujutu/index-e.html], and Grant-in-Aids from Ministry of Education, Culture, Sports, Science, and Technology of Japan [http://www.jsps.go.jp/english/e-grants/index.html]; grants from the Ministry of Health, Labor and Welfare of Japan [http://www.mhlw.go.jp/english/policy/other/research-projects/index.html]; and Core Research for Evolutional Science and Technology (CREST) from the Japan Science and Technology Agency (JST) [http://www.sss.jst.go.jp/english/index.html]. The funders had no role in study design, data collection and analysis, decision to publish, or preparation of the manuscript.

**Competing Interests:** The authors have declared that no competing interests exist.

* E-mail: sobueg@med.nagoya-u.ac.jp

## Introduction

Amyotrophic lateral sclerosis (ALS) is a neurodegenerative disease characterized by selective loss of upper and lower motor neurons in the cerebral cortex, brain stem, and spinal cord [1,2]. Many genes have been identified as involved in familial ALS cases, including Cu/Zn-superoxide dismutase-1 (SOD1) [3,4,5]. Approximately 5–10% of ALS cases are familial, and 20% of familial ALS cases are associated with mutations in the SOD1 gene [3]. Several hypotheses for the pathogenesis of ALS have been proposed, including oxidative stress, glutamate excitotoxicity, mitochondrial dysfunction, and neuroinflammation, all of which eventually lead to the death of motor neurons [6,7,8,9]. Many studies using mutant SOD1 transgenic animals have explored the precise cellular mechanisms of motor neuron death; however, no therapeutic drugs have been developed to date except for riluzole, which has only limited effects. Since most cases of ALS are sporadic, the development of ALS drug therapies based on the pathology of sporadic ALS (sALS) is feasible.

Previously, we performed microarray analyses combined with laser-capture microdissection to investigate the gene expression profiles of spinal motor neurons isolated from autopsied patients with sALS [10]. We found altered expression of many genes, including dynactin 1, early growth response-3, acetyl-CoA transporter, death receptor 5, and cyclin C [10,11]. In that study, a 4.41-fold increase in the amount of c-Abl mRNA was detected in the motor neurons of sALS patients [10]. These findings raised the

possibility that upregulation of c-Abl in motor neurons contributes to motor neuron degeneration and that activation of this pathway may be one of the pathologic features of ALS.

c-Abl is a ubiquitous non-receptor tyrosine kinase that was originally identified as the cellular homolog of the v-abl gene, an oncogene carried by the Abelson murine leukemia virus [12]. Bcr-Abl hybrid protein, which is one of the oncogenic forms of c-Abl fusion kinase, causes chronic myelogenous leukemia (CML) and Philadelphia chromosome-positive adult acute lymphoblastic leukemia (Ph+ALL) [13,14]. The kinase activity of c-Abl is regulated by phosphorylation. Tyrosine 245 (Tyr245) and tyrosine 412 (Tyr412) are well-established regulatory phospho-tyrosine residues that are required for c-Abl activation [15]. In response to various stimuli, c-Abl regulates cytoskeletal rearrangement, cell migration, cell-cell adhesion, cell proliferation, and apoptosis [16,17,18,19,20]. On exposure to stressors, such as DNA damage or oxidative stress, c-Abl has been implicated in cell growth arrest and caused apoptotic cell death in association with p73 [21,22], PKC delta [23], and CDK5 [24,25]. Recently, neural functions of c-Abl have also been described: c-Abl participates in neuronal development and neurite outgrowth [26,27], and has also been implicated in the pathogenesis of Alzheimer's disease [28,29].

In the present study, we investigated c-Abl activation in a mutant SOD1 transgenic ALS mouse model and in sALS patients, and we demonstrated that the c-Abl inhibitor dasatinib has a protective effect on motor neuron degeneration in G93A-SOD1 transgenic ALS mice (G93A mice).

## Results

### Inducible expression of wild-type and mutant SOD1 in NSC-34 cells

To investigate the expression and activity levels of c-Abl in human mutant SOD1-expressing motor neurons, we established an inducible system of NSC-34 cells able to express either human wild-type or mutant (G93A, G85R) SOD1 protein. Western blot analysis confirmed that myc-tagged human SOD1 proteins were induced by doxycycline in these cell lines (Fig. 1A). Myc-tagged human SOD1 demonstrated lower mobility than mouse endogenous SOD1. NSC-34 cells were well differentiated in low-serum medium with extended neuritic processes, a morphological marker of neuronal cell maturation and differentiation [30]. As a motor neuron-mimicking model, we used NSC-34 cells with serum-free medium to measure cytotoxicity. Cell viability was examined using the MTS-based cell proliferation assay at 48 h after the induction of SOD1 proteins, and we found that both G93A and G85R mutant SOD1s significantly decreased cell viability in comparison with wild-type SOD1 ($P<0.05$ for G93A, $P<0.01$ for G85R) (Fig. 1B). The cytotoxicity of mutant SOD1s was also measured by lactate dehydrogenase (LDH) release assay at 48 h after the induction of SOD1 proteins. The results demonstrated that both G93A and G85R mutant SOD1s significantly increased cytotoxicity in comparison with wild-type SOD1 ($P<0.05$ for G93A, $P<0.01$ for G85R) (Fig. 1C).

### c-Abl activation caused by mutant SOD1 in NSC-34 cells

We then investigated whether overexpression of mutant SOD1s influenced the expression of c-Abl. Western blot analysis revealed that the expression of c-Abl was greater in cells expressing mutant SOD1s (G93A and G85R) than cells expressing wild-type SOD1 (Fig. 2A). These differences were much more prominent when phospho-specific antibodies for each of 2 distinct tyrosine residues (Tyr245 and Tyr412) were used for the western blot analysis. Densitometric analysis confirmed that mutant SOD1 significantly increased the expression and phosphorylation of c-Abl ($P<0.05$) (Fig. 2B). Increased c-Abl mRNA expression in cells overexpressing mutant SOD1s was also confirmed by quantitative RT-PCR (Fig. 2C).

### Dasatinib attenuates the cytotoxicity of mutant SOD1s in NSC-34 cells

To examine whether the inhibition of c-Abl kinase influenced the cytotoxicity of mutant SOD1s, we evaluated the effect of dasatinib, a blood-brain barrier (BBB)-permeable c-Abl inhibitor, on c-Abl activity in NSC-34 cells expressing different forms of SOD1. Cells overexpressing SOD1 were treated with increasing concentrations of dasatinib for 24 h and analyzed by western blotting. Dasatinib effectively suppressed the phosphorylation of c-Abl in all cell lines (Fig. 3A). Since dasatinib is a dual c-Abl/c-Src kinase inhibitor [31], in order to clarify the specificity of c-Abl for motor neuronal cytotoxicity, we also performed cell proliferation and cell death assays with SU6656, which preferentially inhibits c-Src compared to c-Abl. SU5666 effectively suppressed the phosphorylation of c-Src in all cell lines (Fig. 3A). Cell viability and cell death assays confirmed that dasatinib significantly reduced the cytotoxicity of mutant SOD1s ($P<0.05$), whereas SU6656 did not (Fig. 3B, C).

### Upregulation and activation of c-Abl in G93A mice

To determine whether c-Abl upregulation also occurs in G93A mice, we measured mRNA and protein levels of c-Abl in the lumbar spinal cords of G93A and control mice at age 10 weeks (pre-symptomatic stage), 14 weeks (symptomatic stage), and 18 weeks (terminal stage) by quantitative RT-PCR and western blot analyses. The protein expression of c-Abl in the lumbar spinal cords of G93A mice was increased as early as 10 weeks compared with control littermates (Fig. 4A). A remarkable increase in the phosphorylation of c-Abl was also evident even at the pre-clinical stage of 10 weeks. The increase in c-Abl protein was paralleled by an induction of c-Abl mRNA in the spinal cords of G93A mice (Fig. 4B). Consistent with the western blot analyses and quantitative RT-PCR, immunoreactivity for c-Abl and phosphorylated c-Abl (Tyr245 and Tyr412) was increased in the lumbar spinal neurons of G93A mice compared with those of control littermates (Fig. 4C). We quantified the signal intensity of phosphorylated c-Abl immunofluorescence in motor neurons (Tyr412 and Tyr245) using Image J software. Phosphorylated c-Abl immunoreactivity in G93A mice was significantly increased compared to control mice with both antibodies ($P<0.01$), which indicated that c-Abl was activated at an early stage of disease in this mouse model of ALS (Fig. S1).

### The effect of dasatinib on survival and disease progression in G93A mice

Survival of G93A mice was improved by dasatinib at a dose of 25 mg/(kg·day) compared with vehicle treatment ($P<0.01$, 25 mg/(kg·day) vs. vehicle), whereas a lower dose of dasatinib (5 mg/(kg·day)) had no significant effect on life span (Fig. 5). Weight loss was also ameliorated by dasatinib at a dose of 25 mg/(kg·day) compared with vehicle treatment (Fig. 5, 2-way ANOVA, $P<0.01$, 25 mg/(kg·day) vs. vehicle). The administration of dasatinib at 25 mg/(kg·day) similarly alleviated motor dysfunction measured by grip strength (2-way ANOVA, $P<0.01$, 25 mg/(kg·day) vs. vehicle). Dasatinib did not significantly ameliorate the physical function assessed by rotarod, although a beneficial tendency was observed. Dasatinib did not alter the neuromuscular

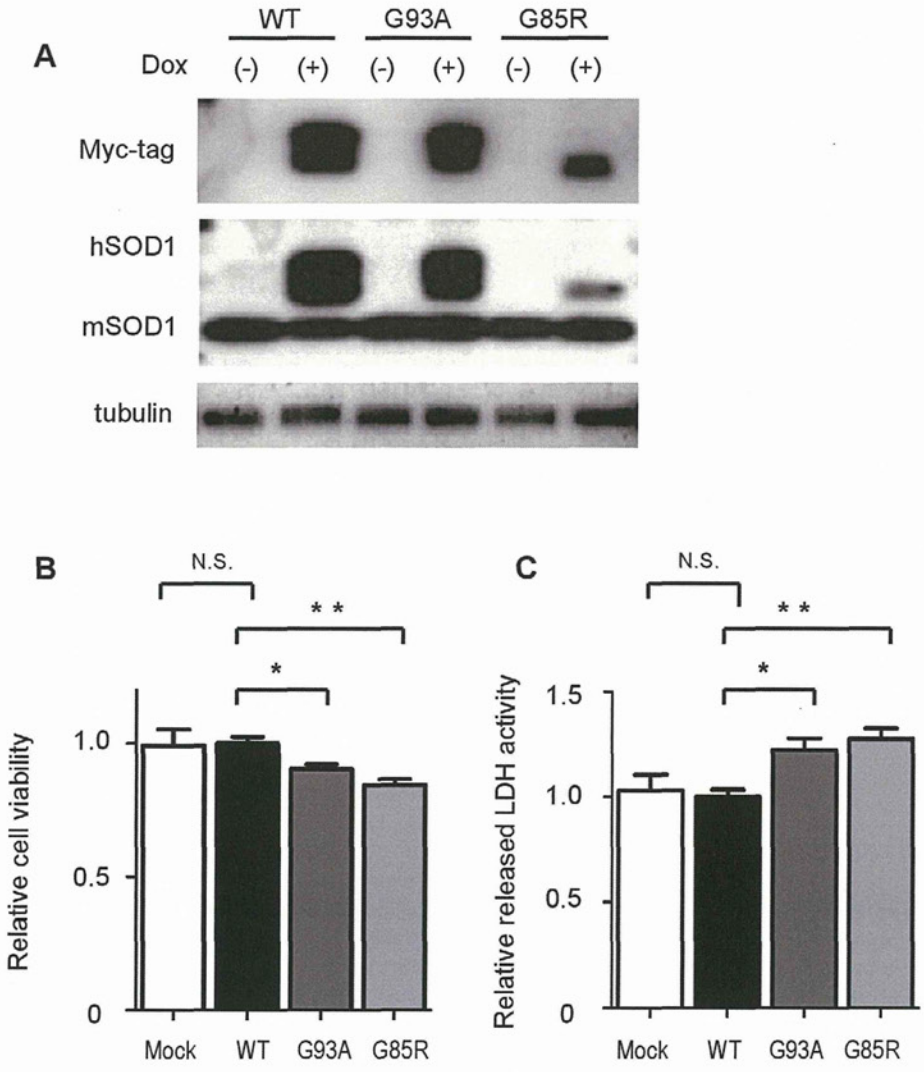


**Figure 1. Inducible expression system of wild-type and mutant SOD1s in NSC-34 cells.** A: NSC-34 cells were stably transduced with an inducible lentivirus expressing human Myc-tagged wild-type or mutant SOD1 protein. Cells were cultured with or without doxycycline (Dox, 2 μg/ml) for 48 h to induce SOD1 protein. Tubulin is shown as a loading control. hSOD1 and mSOD1 indicate human SOD1 and mouse endogenous SOD1, respectively. B: Cell viability assay based on the MTS method showed that overexpression of both types of mutant SOD1, G93A and G85R, caused cytotoxicity in serum-free culture medium. Mock indicates mock-transfected NSC-34 cells. Data are presented as mean ± SEM. Statistics were evaluated using 1-way ANOVA with Dunnett's post-hoc test. *$P<0.05$, **$P<0.01$ C: Cytotoxicity detection assay using the LDH release method revealed that overexpression of both types of mutant SOD1, G93A and G85R, caused cytotoxicity in serum-free culture medium. Data are presented as mean ± SEM. Statistics were evaluated using 1-way ANOVA with Dunnett's post-hoc test. *$P<0.05$, **$P<0.01$.
doi:10.1371/journal.pone.0046185.g001

function or body weight of non-transgenic littermates at any of the doses tested (data not shown).

## The effect of dasatinib on motor neuron survival and innervation status of neuromuscular junctions (NMJs) in G93A mice

Paraffin-embedded sections of the lumbar spinal cord (L1-3) from 120-day-old mice were analyzed immunohistochemically using anti-choline acetyltransferase (ChAT) antibody (Fig. 6A). The number of ChAT-positive motor neurons in the lumbar spinal cord was significantly preserved in mice treated with dasatinib at doses of 15 mg/(kg·day) or higher compared with vehicle-treated control mice ($P<0.05$) (Fig. 6B). To evaluate changes in the size of ChAT-positive motor neurons, we quantified the cell body areas of ChAT-positive motor neurons using Image J software. The size of motor neurons in dasatinib-treated mice was significantly preserved compared to vehicle-treated controls ($P<0.05$) (Fig. 6C). To investigate the innervation status of neuromuscular junctions (NMJs), frozen quadriceps femoris specimens were collected from 120-day-old mice and stained with alpha-bungarotoxin (BuTX) (red) and anti-synaptophysin (green) or anti-SMI31 (green) antibodies (Fig. 6D). We observed BuTX-positive NMJs (treated and control groups; n = 3 mice per group, 100 NMJs per mouse) using confocal laser scanning microscopy and counted double- (red and green) or single (red)-immunostained NMJs. Figure 6E summarizes the ratio of double-immunostained (innervated) NMJs to total NMJs. Dasatinib significantly ameliorated the destruction of NMJ innervation in G93A mice at doses of 5, 15, and 25 mg/(kg·day) compared to vehicle treatment ($P<0.05$) (Fig. 6E).